EFFECTS OF RADIAL-DENSITY AND CURRENT PROFILES ON PRS DYNAMIC MASS AND IMPLODED ENERGY*

D. Mosher, R. J. Commisso, and B.V. Weber
Pulsed Power Physics Branch, Plasma Physics Division
Naval Research Laboratory, 4555 Overlook Ave. SW, Washington DC 20375-5346

Abstract
The line mass and implosion energy inferred from the PRS implosion time and load current depend on the shapes of gas-puff radial-density and current-history profiles. Snowplow calculations with various density and current profiles are used to determine the dependence of these quantities on the profile shapes. Our results demonstrate the importance of using accurate experimental density and current profiles with radiation-scaling analyses.

I. INTRODUCTION

The line mass m_0 and implosion energy E_w inferred from the plasma radiation source (PRS) implosion time and load current depend on the shapes of gas-puff radial-density and current-history profiles. For long implosion times and high photon energy, such as considered for the Decade Quad PRS driver [1], computed K-shell yields can depend sensitively on these quantities [2]. Here, snowplow calculations with various density and current profiles are used to determine the dependence of m_0 and E_w on their shapes. As part of this analysis, a ballistic-transport model is developed to determine realistic density profiles from gas-puff-nozzle parameters.

Analytic forms relating m_0 to the density- and current-profile shapes are found when a mass-averaged radius replaces the nominal outer radius of the density profile. It is shown that small experimental deviations from the commonly-used linearly-rising current can produce factor-of-two errors in calculated dynamic mass, and that diffuse density profiles (without well-defined current-initiation radii) can have surprisingly-large uncertainties in implosion energy. Such results demonstrate the importance of using accurate experimental density and current profiles with radiation-scaling analyses [2, 3].

II. CALCULATIONS AND DISCUSSION

Radial snowplow implosions of a PRS with initial radial line-mass distribution m(r) g/cm driven by an applied current I(t) A are described by

$$\frac{d}{dt}\left\{\left[m_0 - m(R)\right]\frac{dR}{dt}\right\} = -\frac{I^2}{100R} \quad , \tag{1}$$

where R(t) is the snowplow radius. Scaling Eq. (1) leads to

$$t_{imp} = C_t \frac{m_0^{1/2} R_c}{I_0} \quad . \tag{2}$$

where t_{imp} is the implosion time, R_c is a characteristic radius, and I_0 is the maximum current during implosion. The quantity C_t varies with the shapes of the density and current profiles, but is insensitive to the value of stagnation radius $R_f = R(t_{imp})$. Figure 1 shows these dependences in DM2 long-implosion-time, argon-gas-puff experiments using annular and solid-fill nozzles [4].

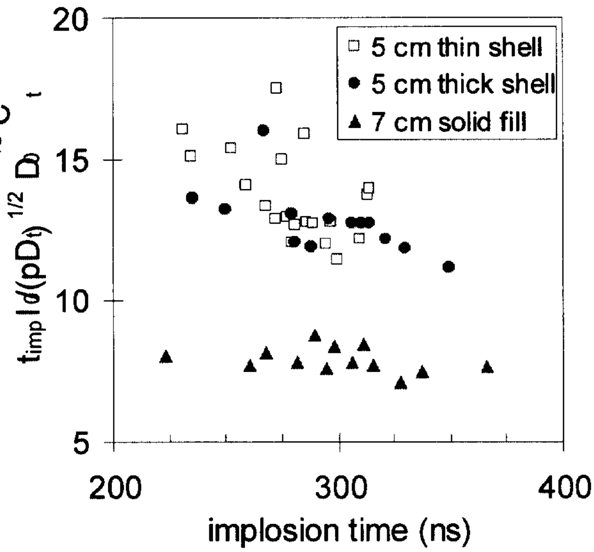

Figure 1. Variation of implosion-time factor with implosion time for three DM2 nozzle geometries.

In Fig. 1, m_0 is taken to be proportional to the product of nozzle pressure p and throat diameter D_t for each shot, while the mean nozzle diameter D_0 determines R_c. These data, and similar data from experiments carried out on HAWK [5], show that calculating load mass from the implosion time depends on the density distribution and, through its variation with implosion time, current shape.

For long-implosion-time experiments such as those on DM2 and HAWK (where a weak current dip at stagnation is observed), a linear current rise to a flat top can be used to characterize current profiles. Designating t_c as the time when the current changes from rising to constant, t_c/t_{imp} is in the range 0.65-0.85 for DM2, and in the range 0.2-0.6 for Hawk operating with a plasma opening switch (POS).

This current profile is first used with a variable-width, uniform-density annulus (UFA) defined by n = constant for $R_1 \leq R \leq R_0$, and zero otherwise. Results of these snowplow computations can be summarized by two mass factors ($\sim 1/C_t^2$) defined by

Report Documentation Page

Form Approved
OMB No. 0704-0188

1. REPORT DATE	2. REPORT TYPE	3. DATES COVERED
JUN 1999	**N/A**	**-**

4. TITLE AND SUBTITLE
Effects Of Radial-Density And Current Profiles On Prs Dynamic Mass And Imploded Energy

5a. CONTRACT NUMBER
5b. GRANT NUMBER
5c. PROGRAM ELEMENT NUMBER

6. AUTHOR(S)

5d. PROJECT NUMBER
5e. TASK NUMBER
5f. WORK UNIT NUMBER

7. PERFORMING ORGANIZATION NAME(S) AND ADDRESS(ES)
Pulsed Power Physics Branch, Plasma Physics Division Naval Research Laboratory, 4555 Overlook Ave. SW, Washington DC 20375-5346

8. PERFORMING ORGANIZATION REPORT NUMBER

9. SPONSORING/MONITORING AGENCY NAME(S) AND ADDRESS(ES)

10. SPONSOR/MONITOR'S ACRONYM(S)

11. SPONSOR/MONITOR'S REPORT NUMBER(S)

12. DISTRIBUTION/AVAILABILITY STATEMENT
Approved for public release, distribution unlimited

13. SUPPLEMENTARY NOTES
See also ADM002371. 2013 IEEE Pulsed Power Conference, Digest of Technical Papers 1976-2013, and Abstracts of the 2013 IEEE International Conference on Plasma Science. Held in San Francisco, CA on 16-21 June 2013. U.S. Government or Federal Purpose Rights License.

14. ABSTRACT
The line mass and implosion energy inferred from the PRS implosion time and load current depend on the shapes of gas-puff radial-density and current-history profiles. Snowplow calculations with various density and current profiles are used to determine the dependence of exthese quantities on the profile shapes. Our results demon- periments strate the importance ofusing accurate experimental density and current profiles with radiation-scaling analyses.

15. SUBJECT TERMS

16. SECURITY CLASSIFICATION OF:			17. LIMITATION OF ABSTRACT	18. NUMBER OF PAGES	19a. NAME OF RESPONSIBLE PERSON
a. REPORT	b. ABSTRACT	c. THIS PAGE			
unclassified	**unclassified**	**unclassified**	**SAR**	**4**	

Standard Form 298 (Rev. 8-98)
Prescribed by ANSI Std Z39-18

$$m_0(\mathrm{mg/cm}) = C_m \cdot \left[\frac{t_{imp}(\mu s) I_0(\mathrm{MA})}{R_0(\mathrm{cm})}\right]^2 , \quad (3)$$

$$m_0(\mathrm{mg/cm}) = C_m' \cdot \left[\frac{t_{imp}(\mu s) I_0(\mathrm{MA})}{\langle R\rangle(\mathrm{cm})}\right]^2 , \quad (4)$$

where

$$\langle R\rangle = \int n(r) r^2 dr \Big/ \int n(r) r dr = \frac{2R_0}{3} \cdot \frac{1-(R_1/R_0)^3}{1-(R_1/R_0)^2} \quad (5)$$

is a mass-averaged radius, and the right-hand side of Eq. (5) is for the UFA density distribution. The variations of C_m and C_m' with annulus width $\Delta = R_0 - R_1$ are shown in Fig. 2 for a linear current rise ($t_c = t_{imp}$). The relative constancy of C_m' suggests that the factor-of-two variation in m_0 associated with density-profile shape can most-easily be accounted for by using Eq. (4), and this form is displayed in what follows. Knowledge of the density profile is still required to determine m_0 from <R>. This procedure was used in HAWK neon gas-puff experiments [5] to achieve agreement with interferometer measurements [6].

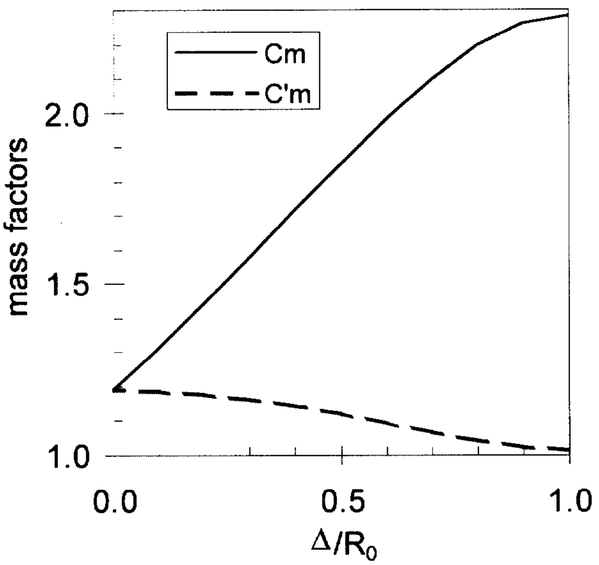

Figure 2. Variation of the mass factors with UFA-model annulus width for a linear current rise.

Figure 3 plots the variation of C_m' with current-profile shape for three values of Δ/R_0. The figure shows that m_0 depends sensitively on the current shape, so that even the modest DM2 flat-top current can increase the mass inferred from a linearly-rising current by a factor of 2. C_m' remains nearly constant with density-profile shape. The mass-factor in the figure is well fit by

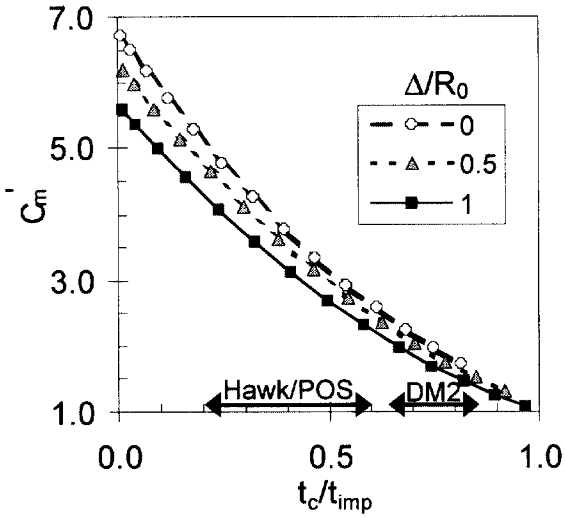

Figure 3. Variation of C_m' with current shape for various UFA density-profile widths.

$$C_m' = 10^3\left[12 + 1.3\frac{\Delta}{R_0} + 10\left(\frac{t_c}{t_{imp}}\right) + 8\left(\frac{t_c}{t_{imp}}\right)^3\right]^{-2} . \quad (6)$$

A ballistic-transport (BT) model can be used to determine more-accurate density profiles from gas-puff-nozzle parameters [6]. For this model,

$$n(r,z) = \frac{N}{\pi(z\theta_d)^2}\exp\left[-\frac{r^2+(R_N - z\theta_t)^2}{(z\theta_d)^2}\right] I_0\left[\frac{2r(R_N - z\theta_t)}{(z\theta_d)^2}\right] \quad (7)$$

In Eq. (7), N is the line density, θ_d is the divergence angle of gas escaping from the nozzle, z is the distance from the nozzle, R_N is the nozzle radius, θ_t is the nozzle tilt angle, and I_0 is the Bessel function. Experimental density contours measured with interferometry at various distances from the nozzle compare favorably with those predicted by the BT model [6] using single values for the three nozzle parameters. Partial results are shown in Fig. 4.

For the implosion calculations of interest here, BT density profiles can be specified in terms of a single parameter δ/R_0 as follows.

$$R_0 = R_N - z\theta_t \quad ; \quad \delta = z\theta_d$$

$$\frac{\pi R_0^2 n}{N} = \left(\frac{R_0}{\delta}\right)^2 \exp\left\{-\left(\frac{R_0}{\delta}\right)^2\left[1+\left(\frac{r}{R_0}\right)^2\right]\right\} I_0\left[2\frac{r}{R_0}\left(\frac{R_0}{\delta}\right)^2\right] \quad (8)$$

For $\delta/R_0 \ll 1$, the radial density distribution is a thin Gaussian annulus centered about R_0. For $\delta/R_0 > 1$, i.e. for $z > R_N/(\theta_d + \theta_t)$, the profile approaches a Gaussian of expanding width δ about the axis of symmetry. Note that for BT distributions, R_0 represents a radius inside the distribution and does not characterize the outside edge, which is not well-defined for such diffuse distributions. The mass-averaged radius from Eq. (5) is well fit by

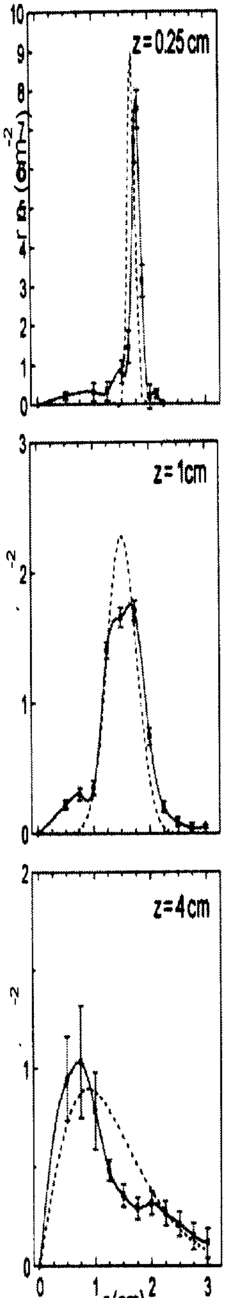

Figure 4. Comparison of BT model (dashed) and measured (solid) arial-density distributions at three axial locations.

$$\langle R\rangle = \sqrt{R_0^2 + \frac{\pi}{4}\delta^2} \quad . \tag{9}$$

The mass factor C_m' (δ/R_0, t_c/t_{imp}) can be determined for these more-realistic density profiles. Related phenomena, such as zippering, can then be determined as functions of of the nozzle parameters R_N, θ_d, and θ_t.

Figure 5 plots the variation of C_m' with current-profile shape for various values of δ/R_0. BT density-profile mass-factor variations with current shape are seen to be

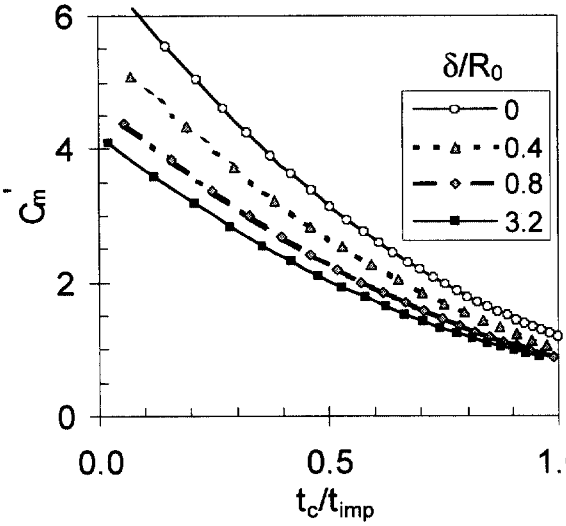

Figure 5. Variation of BT-model mass-factor with current shape for various δ/R_0 values.

similar to those of UFA profiles, though the variations of m_0 with density profile through Eq. (4) is different because of the different dependence of $\langle R\rangle$ on radial shape. For BT profiles, $\langle R\rangle > R_0$ because of mass contributions in the tail at larger radius. For UFA profiles, $\langle R\rangle < R_0$ since all mass is at smaller radius.

The $\delta/R_0 = 0$ curve in Fig. 5 is the same as that of the UFA model with $\Delta/R_0 = 0$. For large values of δ/R_0, the shape of the density profile remains Gaussian and the C_m' values are the same as those of the 3.2 curve. However, the corresponding m_0 values continue to change because $\langle R\rangle$ scales with δ as in Eq. (9). The curves of Fig. 5 are well fit by the form of Eq. (6) with $12 + 1.3\Delta/R_0$ replaced by $11.8 + 3.5(\delta/R_0)$, 10 replaced by $9.6 + 1.9(\delta/R_0)$, and 8 replaced by $7.5 + \delta/R_0$.

For snowplow implosions, the implosion energy E_W exceeds the slug-model kinetic energy and can be determined from the electrical characteristics of the PRS load. For I(t) in MA and load inductance L(t) in nH/cm

$$E_W(\mathrm{kJ/cm}) = \int_0^{t_{imp}} \left(\frac{I^2}{2} \frac{dL}{dt} \right) dt = -\int_0^{t_{imp}} \left(I^2 \frac{1}{R} \frac{dR}{dt} \right) dt \tag{10}$$

If the initial radius of current flow R_i is well defined, E_W can be written [2]

$$E_W(\mathrm{kJ/cm}) = \gamma I_0^2(\mathrm{MA}) \ln\left(\frac{R_i}{R_f} \right) \quad , \tag{11}$$

where γ depends on the density and current shapes. When $\gamma = 1$, Eqs. (10) and (11) yield $I^2\Delta L/2$ for implosion at constant current ($t_c = 0$). Figure 6 shows the variation in γ with current shape for UFA-model density distributions. The implosion energy varies by less than 10% with density distribution and can be determined with accuracy for the experimental current profile [2]. Values of γ for short-

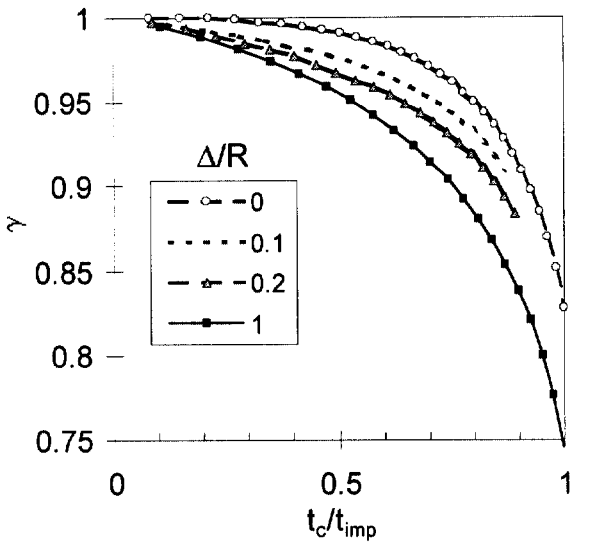

Figure 6. Variation of energy factor with current shape for various annular width in the UFA model.

implosion-time current profiles with strong dips near stagnation will be smaller by about 0.1.

For diffuse profiles where R_i may not be well-defined, γ may be replaced by $e_W = E_W(kJ/cm)/I_0^2(MA)$, computed from Eq. (10) with the assumption that the current moves with the snowplow. Results for BT density profiles are

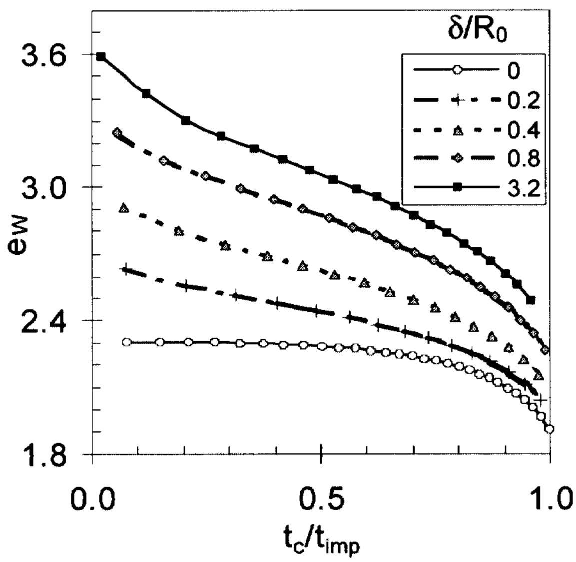

Figure 7. Variation of implosion energy with current shape for various values of δ/R_0 and $R_f = \langle R\rangle/10$.

shown in Fig. 7 for the case $R_f = \langle R\rangle/10$. Note that the compression ratio varies with δ/R_0 since $\langle R\rangle$ varies with the profile shape. For UFA profiles, e_W increases with Δ because compression increases like $10R_0/\langle R\rangle$, and $\langle R\rangle$ decreases with Δ. For the diffuse BT profiles, e_W increases with δ because compression increases like $10R_i/\langle R\rangle$, and R_i, far out on the tail of the distribution, increases with δ faster than $\langle R\rangle$ does. The BT implosion energy increases at small t_c/t_{imp} because the current is established at early times when the snowplow is still at large radius. Because of the low-density wings, the diffuse-profile implosion energy depends more sensitively on details of both the density and current distributions. This can lead to large uncertainties in the calculation of E_W if the experimental profiles are not taken into account.

III. SUMMARY OF RESULTS

The dependence of dynamic mass m_0 and implosion energy E_W on the shapes of the radial-density and current-history profiles has been systematically quantified. In addition to a simple, uniform-fill, fat-annulus density profile, a generally-useful, ballistic-transport model has been developed for this analysis and benchmarked against interferometer measurements to determine more-realistic density profiles from gas-puff-nozzle parameters. Analytic forms relating m_0 to the density- and current-profile shapes are found when a mass-averaged radius replaces the outer radius of the density distribution. Small experimental deviations from the commonly-used linearly-rising current have been shown to produce factor-of-two errors in dynamic mass. Also, diffuse density profiles without well-defined current-initiation radii can lead to surprisingly-large errors in implosion energy. As computed K-shell yields can depend sensitively on m_0 and E_W, our results demonstrate the importance of using accurate experimental density and current profiles with radiation-scaling analyses.

IV. REFERENCES

*Work supported by DTRA.

[1] P. Sincerny, et al., "Decade Quad design and testing status," *Proc. 11th International Pulsed Power Conf.*, I. Vitkovitsky and G. Cooperstein, eds., Baltimore, 1997, p.698.

[2] D. Mosher, N. Qi, and M. Krishnan, "A two level model for K-shell radiation scaling of the imploding Z-pinch plasma radiation source," *IEEE Trans. Plasma Sci.* **26**, 1052(1998).

[3] J.W. Thornhill, K.G. Whitney, J. Davis, and J.P. Apruzese, "Investigations of K-shell emission from moderate-Z, low-η (–velocity) Z-pinch implosions," *J. Appl. Phys.* **80**, 710(1996).

[4] J. Riordan, et al., "Long Implosion Plasma Radiation Source," *1998 ICOPS Conf. Record Abstracts*, 98CH36221, p244.

[5] R.J. Commisso, et al., "Results of radius scaling experiments and analysis of Ne K-shell radiation data from an inductively-driven Z-pinch," *IEEE Trans. Plasma Sci.* **26**, 1068(1998).

[6] B.V. Weber, et al., "Measurements of gas distributions from PRS Nozzles," *Proc. 1997 Dense Z-Pinch Conf., AIP Conf. Proc. 409*, 459(1997).